RESEARCH ARTICLE

Caldera faults capture and deflect inclined sheets: an alternative mechanism of ring dike formation

John Browning · Agust Gudmundsson

Abstract The subsurface structures of caldera ring faults are often inferred from numerical and analog models as well as from geophysical studies. All of these inferred structures need to be compared with actual ring faults so as to test the model implications. Here, we present field evidence of magma channeling into a caldera ring fault as exhibited at Hafnarfjall, a deeply eroded and well-exposed 5-Ma extinct volcano in western Iceland. At the time of collapse caldera formation, over 200 m of vertical displacement was accommodated along a ring fault, which is exceptionally well exposed at a depth of approximately 1.2 km below the original surface of the volcano. There are abrupt changes in the ring fault attitude with depth, but its overall dip is steeply inward. Several inclined sheets within the caldera became arrested at the ring fault; other sheets became deflected up along the fault to form a multiple ring dike. We present numerical models showing stress fields that encourage sheet deflection into the subvertical ring fault. Our findings provide an alternative mechanical explanation for magma channeling along caldera ring faults, which is a process likely to be fundamental in controlling the location of post-caldera volcanism.

J. Browning (✉) · A. Gudmundsson
Department of Earth Sciences, Royal Holloway, University of London, Egham TW20 0EX, UK
e-mail: john.browning.2012@live.rhul.ac.uk

Introduction

Many ring faults around the world are intruded by dikes (e.g., Smith and Bailey, 1968; Johnson et al., 2002). These dikes are believed to have been emplaced either during the injection of magma during collapse caldera formation (Anderson, 1936; Sparks, 1988; Walter, 2008) or incrementally through many injections along the ring fault (Saunders, 2001). The common assumption, based on Anderson's (1936) model, is that ring dikes are injected directly into the ring fault at its contact with the magma chamber.

Dikes and sheets commonly intrude pre-existing weaknesses such as joints (Delaney et al., 1986) and faults (Gudmundsson, 2011; Magee et al., 2013; Bedard et al., 2012). While there are numerous examples of well-studied ring faults, for example Glencoe caldera (Clough et al., 1909; Kokelaar, 2007) and Hannegan caldera (Tucker et al., 2007) as well as many others (see Lipman 1984), observations of well-exposed ring faults and ring dikes in the same vertical cross section at depth are extremely rare. As such, the mechanics of magmatic interaction with caldera faults is still poorly understood.

Many calderas experience post-collapse resurgence which may culminate in eruptive activity. Commonly, post-caldera volcanism concentrates spatially above the vertical extent of a caldera ring fault (Geyer and Martí 2008; Saunders, 2004). Therefore, understanding the subsurface structure of caldera ring faults is important for identifying the location and timing of renewed volcanic activity within active calderas. Caldera ring faults have traditionally been studied using analog (e.g., Acocella et al., 2000; Acocella, 2007; Geyer et al., 2006; Holohan et al., 2005; Kennedy et al., 2004), numerical (e.g., Gudmundsson, 1998; Hardy, 2008), and analytical methods (e.g., Gudmundsson, 1998), with the subsurface structure often inferred from such models, as well as from seismicity (e.g., Ekstrom, 1994), geodetic studies (e.g., Jonsson, 2009),

and near-surface observations (e.g., Geshi et al., 2002; Troll et al. 2002). Caldera ring faults are primarily subvertical dip-slip shear fractures, although in some cases, the faults accommodate an oblique slip (Holohan et al., 2013). Whether a caldera ring fault dips inward or outward from the center of subsidence is a long-debated and contentious issue (Gudmundsson and Nilsen, 2006; Burchardt and Walter, 2010; Geyer and Marti, 2014). For example, Branney (1995) suggests that most ring faults dip outward, whereas observations from the collapse of Miyakejima, Japan, in 2000 (Geshi et al., 2002; Burchardt and Walter, 2010) and Piton de la Fournaise, La Reunion, in 2007 (Michon et al., 2009) indicate both inward- and outward-dipping ring faults. The use of near-surface observations of ring faults (e.g., Michon et al., 2009) may be misleading as caldera walls are subject to mass wasting and erosion (Lipman, 1997). Furthermore, it may be difficult to infer correctly the subsurface structure from surface observations because the fault-generating local stresses are likely to vary with depth in the volcanic edifice, thereby affecting the overall geometry of the fault structure (Gudmundsson, 2011).

Here, we present field data and numerical models which show that dikes and sheets can become deflected at and along a ring fault, the deflection being primarily due to the difference in material properties between (and within) the fault zone and the host rock. These observations and associated modeling provide an alternative mechanism for the formation of ring dikes.

A well-exposed caldera ring fault in western Iceland

Hafnarfjall is an inactive and deeply eroded 5-Ma-old central volcano (stratovolcano with a caldera) in western Iceland. The volcano is composed of a predominantly basaltic lava pile overlain by brecciated andesite and andesitic lava, as described in detail by Franzson (1978) (Fig. 1). The volcano originally formed in the southwest volcanic zone of Iceland but subsequently drifted, through crustal spreading, 40–50 km (Gautneb et al., 1989) to the west-northwest of the rift zone. Hafnarfjall therefore offers the opportunity to study a caldera formed in a divergent plate boundary setting. We estimate that glacial erosion has removed the uppermost parts of the volcano based on the assumptions of Walker (1960) and Johannesson (1975) who used zonation of amygdale minerals to estimate the level of erosion in a nearby area. Hafnarfjall volcano contains numerous inclined sheets, predominantly basaltic, which dip on average at around 65°, trend NE, and have thicknesses that are commonly about 1 m or less (Gautneb et al., 1989). The thickest sheets, however, reach about 10 m and tend to be composed of rhyolite. Many of these intrusions in Hafnarfjall are highly altered, and it is often difficult to discern characteristic intrusive features such as chilled selvages and cooling jointing. In Fig. 2, we show several dikes and inclined sheets ranging in thickness from

Fig. 1 Geological map of Hafnarfjall central volcano, located in western Iceland, approximately 50 km northwest of the active volcanic zone (*AVZ*). The ring fault of the 7.5×5-km NW-SE elongated caldera is shown. Study area is marked with a *yellow star*. Modified after Franzson (1978)
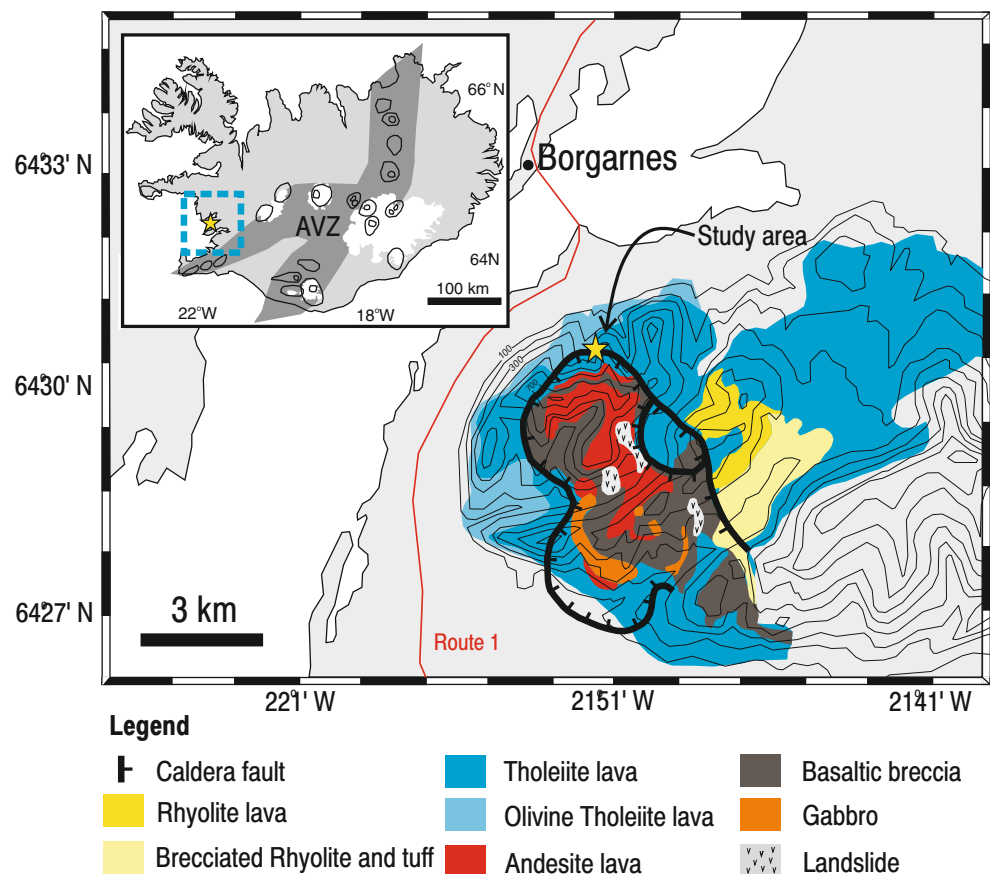
2.5 m (Fig. 2a) to 3 cm (Fig. 2c). They are all clearly intrusions which are discordant to bedding; however, very few display characteristic chilled selvages or discernible horizontal fracture patterns.

At around 4.6 Ma, Hafnarfjall experienced a major collapse event, forming part of a NW-SE elongated caldera approximately 7.5×5 km in diameter (Franzson, 1978). The most striking evidence of this collapse is the exposed ring fault in a gulley, oriented roughly NW-SE, at the northernmost margin of the caldera, as shown in Fig. 3. At this locality, an E-W trending segment of the ring fault can be observed in a vertical cross section for 200 m along dip and around 700 m along strike (Fig. 3a). Here, the ring fault cuts a 300-m-thick lava pile composed of 2–5-m-thick flows of basaltic tholeiite. Around the outer caldera margin, lavas dip 15° S, whereas the dip of lavas which constitute the caldera block increases to ~35° S. This implies that the caldera block has tilted during faulting. Dips of intra-caldera lavas also increase with depth toward the center of the caldera, i.e., individual lava layers at the outcrop base exhibit a steeper dip than those near the present-day surface. The caldera fault can be traced in several localities as mapped by Franzson (1978) and shown in Fig. 1 as a single fault plane with displacement in excess of 100 m. The exposure described in detail here indicates a throw in excess of 200 m, although the normal fault offset is considered a minimum and is based on the inability to trace individual lava flow layers horizontally, across the entire vertical section. As mentioned, the vertical section is 300 m, although individual lava layers can only be obviously discerned for approximately 200 m of this section.

The studied vertical section of the ring fault does not display a constant attitude. This finding is in contrast to those of many models on ring fault formation that often predict a simple inward- or outward-dipping trend (Acocella, 2007). Instead, the fault alternates in dip between 85 N–90° and 85 S–90°, suggesting that a number of stress perturbations occurred during fracture propagation. Such subtle changes in fault attitude are unlikely to be detected in models unless a heterogeneous, in particular, a layered, edifice is considered. On average, the fault has a normal trend and dips steeply inward, at ~85° S.

Steep-sided slopes surrounding the fault exposure limit observations to the base of two gullies and, from a distance, to a parallel topographic high (Fig. 3a, b). At the base of the caldera fault (Fig. 4) are five thin (<0.7 m) basaltic, but highly altered, dikes. Thin (0.5–1 cm) mineral veins separate some of the individual intrusions, as shown in Fig. 4c. Surprisingly, no breccia or fault gouge is found along the main fault plane. We interpret the dikes within the fault plane as ring dikes and now refer to them as such throughout. In Fig. 4b, two ring dikes can be clearly observed within the fault plane; the northernmost dike strikes N086° E, and it becomes offset around 25 m vertically in the pile. The strike of the second dike is variable between approximately 095 and 115 and appears to follow the fault plane. In the intra-caldera lava pile, thin (<1 m) inclined sheets dip between 45 and 75° S, and upon contact with the fault, the sheets either become arrested or change attitude and deflect vertically into the fault. No sheets can be traced from inside of the caldera margin, across the fault, and to the outside of the caldera.

On the intra-caldera margin, synclinal drag folding indicates a normal sense of dip-slip shear and displacement (see Fig. 3a). The zone of folding extends for approximately 10–15 m horizontally toward the caldera center. In this region, it is difficult to distinguish between individual lava flows, as their

Fig. 2 Examples of sheets and dikes found in the Hafnarfjall lava pile. **a** View southeast toward the caldera ring fault, indicated as a *dashed line*. **b** Dikes and sheets are discernible as discordant linear features within the lava pile, in this example a pair of cross-cutting dikes, the largest and youngest of which is approximately 2.5 m in thickness and dips 65–75° S. Other dikes and sheets are indicated by *red arrows*. **c, d** A 3-cm-thick arrested dike exhibiting a narrow and pointed dike tip. Due to weathering and alteration, it is difficult to observe any chilled selvage or horizontal fracture pattern within the dike; this is common in many of the intrusions in Hafnarfjall
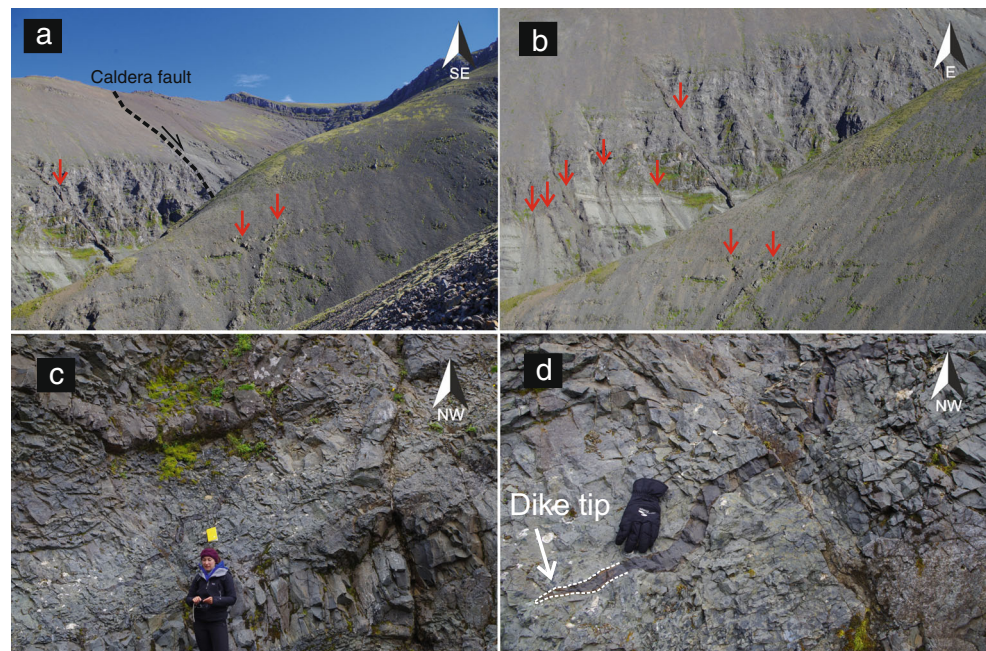
Fig. 3 a Caldera ring fault exhibits a general inward-dipping normal trend, although subtle variations in attitude occur throughout. The height from the base to the top of the fault is ~300 m. Lavas on the inner caldera margin dip more steeply than those outside, and generally dip increases with depth. Several markers are used to infer synclinal drag folding, perhaps the most prominent is a light white tuff which clearly bends into the fault. Displacement is greater than the vertical section, so no horizontal markers can be traced across the fault plane. b Many individual lava layers with thicknesses between 1 and 2 m can be traced to the fault contact on the outer margin; however, most lavas on the inner margin are sufficiently deformed and not discernible. c, d Section of the upper observable part of the fault. Individual dikes shown and numbered are around 1 m thick. (Location 64° 30′ 01″ N 21° 52′ 39″ W)

Sub-vertical ring-dikes within the fault plane

Sheet deflection at fault contact
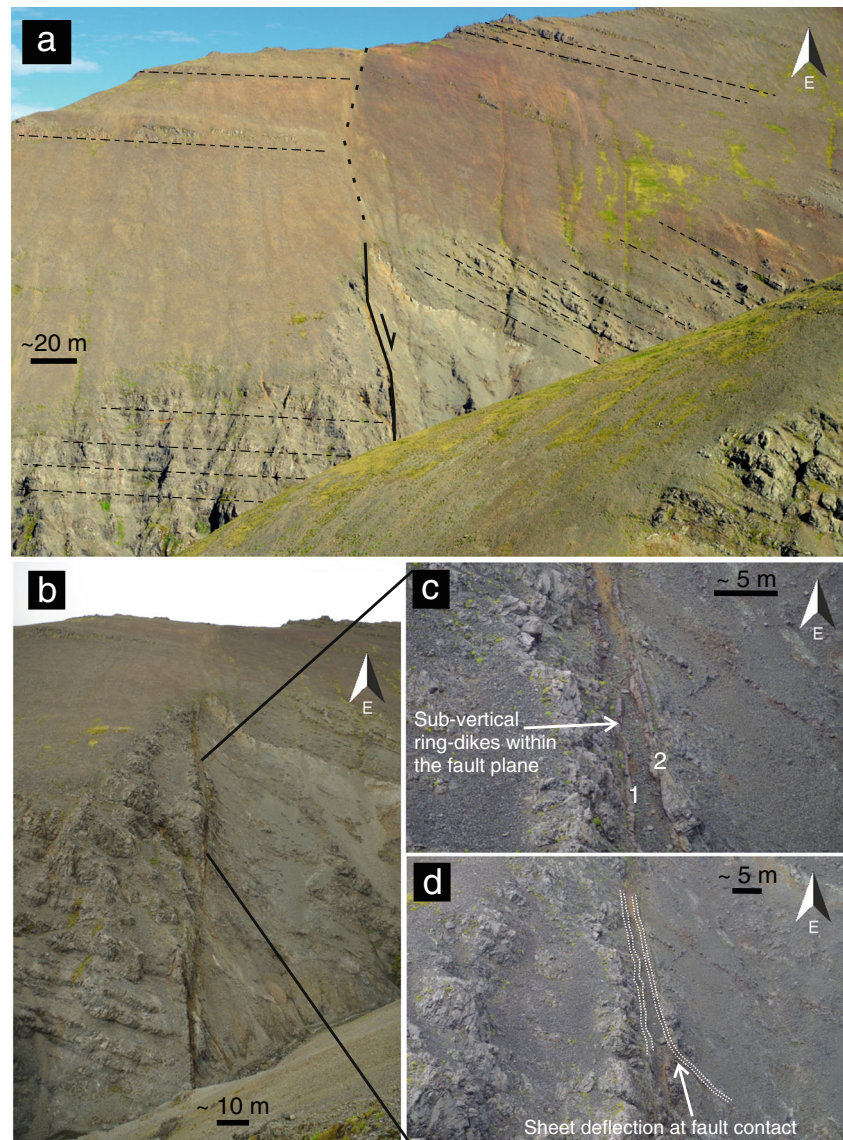
characteristic scoria margins have been sufficiently deformed. There is no indication of reverse-sense displacement or motion on the fault, which is a commonly interpreted mechanism during caldera unrest due to magma intrusion (Acocella et al., 2000; Walter and Troll 2011; Jonsson, 2009). This is important to note, as our later numerical models simulate an overpressured condition, which is of course a requirement for propagating the original sheets described throughout.

Factors influencing the propagation of dikes and sheets

Stress barriers

In order for a sheet to successfully propagate, tensile stress magnitudes should exceed the in situ host rock tensile strength, which is generally between 0.5 and 6 MPa (Amadei and Stephansson, 1997; Gudmundsson, 2011). The direction of propagation is based on Anderson's (1936) theory of sheet and ring dike propagation and on numerous field observations of dikes and sheets which suggest that magmatic fractures will propagate in a direction parallel to the trajectories σ_1 and perpendicular (or normal) to σ_3 (cf. Gudmundsson, 2011). A stress barrier is a layer or unit where the local stress field is unfavorable for the propagation of a particular type of fracture. For example, for a vertically propagating extension fracture, a stress barrier would be a layer where the maximum compressive stress flips to horizontal, a situation which favors dike arrest (Gudmundsson and Phillip, 2006). Both stiff (high Young' modulus) and soft (low Young's modulus, compliant) layers can act as stress barriers (Gudmundsson and Phillip, 2006).

Fig. 4 Base of the outcrop of the ring fault, where four thin ring dikes (<0.7 m) of basaltic composition occupy the subvertical segment (**a**). Two of these dikes are observable in the vertical section (**b**, **c**): one can be traced inside the caldera margin (**d**), several inclinedand sheets strike E-W to NE-SW and dip between 65 and 80° S; at least two of the sheets meet the fault contact higher in the pile
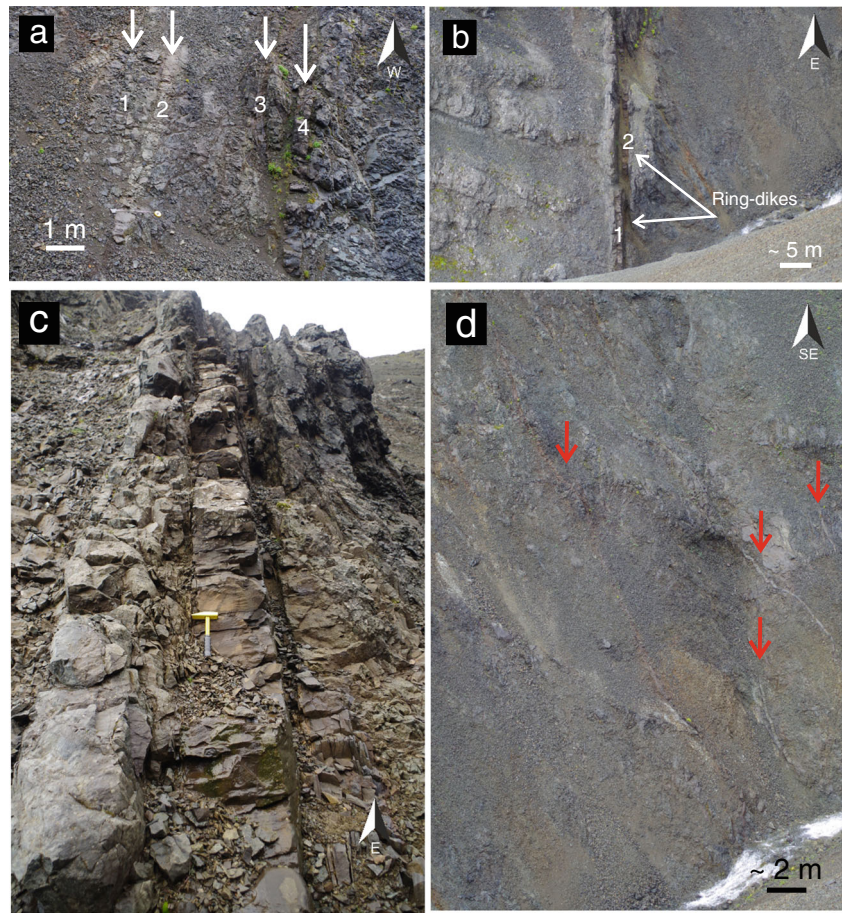
Elastic mismatch

The second mechanism responsible for dike deflection is related to the difference in material properties of the layers hosting, and directly in front of, a propagating fracture and the associated contacts. Dikes and sheets are extension fractures or mode I cracks. However, when such fractures meet and become deflected into a contact or discontinuity, they temporarily become mixed-mode (He and Hutchinson, 1989; Xu et al., 2003). Consider the total strain energy release rate G_{total} in mixed-mode fracture propagation:

$$G_{total} = G_I + G_{II} + G_{III} = \frac{(1-v^2)K_I^2}{E} + \frac{(1-v2)K_{II}^2}{E} + \frac{(1+v)K_{III}^2}{E} \tag{1}$$

G_{I-III} are the energy release rates (Jm^{-2}) of ideal mode I–III cracks (Anderson, 2005; Gudmundsson, 2011), E is the Young's modulus, v is the Poisson's ratio, and K_{I-III} are the stress intensity factors. When the rock layer which hosts the dike or sheet has the same or similar mechanical properties to a rock layer above, then the strain energy release rate for a mode I crack, G_p, reaches a value suitable for fracture extension, which is equal to the material toughness of the layer, Γ_L. Therefore, from Eq. (1), the condition becomes

$$G_p = \frac{(1-v^2)K_I^2}{E} = \Gamma_L \tag{2}$$

However, the dike or sheet will deflect into the discontinuity if the strain energy release rate becomes the same as the material toughness of the discontinuity, Γ_D. Deflection at the discontinuity then occurs when

$$G_d = \frac{(1-v^2)}{E}\left(K_I^2 + K_{II}^2\right) = \Gamma_D \tag{3}$$

It follows that a dike or sheet will continue on the same trajectory, through a discontinuity if (He and Hutchinson, 1989)

$$\frac{G_{\mathrm{d}}}{G_{\mathrm{p}}} < \frac{\Gamma_{\mathrm{D}}(\Psi)}{\Gamma_{\mathrm{L}}} \qquad (4)$$

or become deflected at the discontinuity if

$$\frac{G_{\mathrm{d}}}{G_p} \geq \frac{\Gamma_{\mathrm{D}}(\Psi)}{\Gamma_{\mathrm{L}}} \qquad (5)$$

where Ψ denotes the measure of the relative proportion of mode II to mode I:

$$\Psi = \tan^{-1}\left(K_{\mathrm{II}}/K_{\mathrm{I}}\right) \qquad (6)$$

In Fig. 5, the ratio of $G_{\mathrm{d}}/G_{\mathrm{p}}$ is plotted as a function of α, which represents the Dundurs elastic mismatch parameter and can be presented in the following form (He and Hutchinson, 1989):

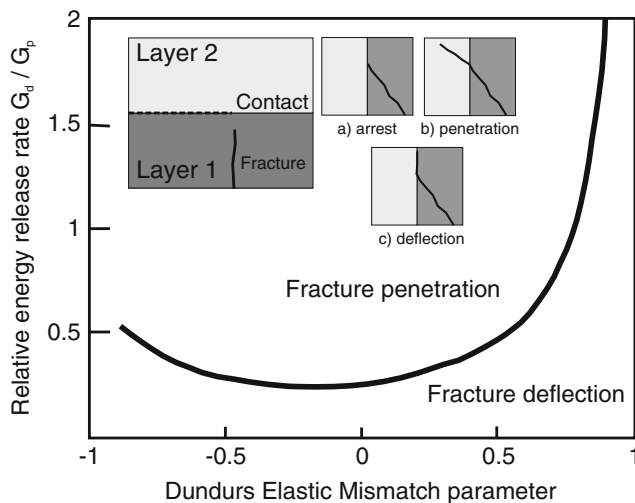$$\alpha = \frac{E_1 - E_2}{E_1 + E_2} \qquad (7)$$

Fig. 5 Conditions for fracture propagation: upon meeting a contact between two layers with contrasting material properties, a fracture will either (*a*) arrest, (*b*) penetrate the contact, or (*c*) deflect at the contact. The ratio of strain energy release rate for fracture deflection (G_d) against fracture penetration (G_p) is plotted as a function of the Dundurs elastic mismatch parameter (α; see text for details). Modified after He et al. (1994)

Here, E denotes the plane strain Young's modulus, and the subscripts 1 and 2 relate to the moduli of the rock above and hosting the dike, respectively. The ratio below the curve in Fig. 5 indicates areas where the deflection of a dike or sheet is favored, whereas those areas above the curve indicate continued propagation with no deflection.

Cook-Gordon mechanism

Experiments on crack propagation have shown that Cook-Gordon debonding is a common mechanism in the delamination of composite materials (Xu et al., 2003; Wang and Xu 2006). It has been shown that the tensile strength ahead of a propagating dike can open up a contact ahead of the dike tip (Gudmundsson, 2011). Such a mechanism is important in where there is an abrupt change in the mechanical properties or rocks across an interface or a contact, particularly when the contact is clearly defined and mechanically weak (with a low tensile strength). However, in a fault zone such as that described previously, the contact between the fault and host rock is not clearly defined. As such, we do not consider this mechanism as important for capturing sheets within the fault, at least initially.

Numerical model setup

To test the proposal that sheets can become arrested at or deflected into a caldera fault, we made several numerical models. In all the models, we calculate the stress field around a 1-m-thick dike subject to an internal magmatic excess pressure of 5 or 10 MPa as the initial loading. The weight of overlying host rock or the overburden pressure is included in the lithostatic stress (Jaeger and Cook, 1979) and is therefore taken into account when considering loading as excess pressure in the sheet (Gudmundsson, 2011).

In the numerical models presented here (Figs. 7, 8, 9, 10, and 11), the focus is on the mechanical properties of the caldera fault zone, namely the stiffness or Young's modulus (E) of the layers that constitute the damage zone and the core of the fault, and the more gently dipping layers through which the sheet propagates. Density and Poisson's ratio are kept constant in all model runs, with values of 2500 kg m^{-3} and 0.25, respectively. We estimate that the damage zone surrounding the ring fault is approximately 15 m thick and occurs predominantly on the southern, down-throw ("hanging wall") side of the fault. The damage zone is qualitatively estimated based on the ability to discern individual lava flows, which on the northern wall can be traced to the fault contact but on the southern wall are highly altered and deformed. This deformation zone is observed laterally south for around 15 m from the fault core, which contains the ring dikes, to a point where

individual lava flow characteristics are discernible. Fault core and damage zones have been recognized and measured on different scales in many areas of Iceland (Gudmundsson et al. 2011). The fault zone is modeled simply as three individual layers of similar thickness but with differing mechanical properties. The models presented are designed to test how the local stress field changes as an inclined sheet (a) approaches a ring fault and (b) becomes captured by the fault.

The sheet is situated perpendicular to the fault zone (see the model setup in Fig. 6). A section of the ring fault is modeled in two dimensions as a series of subvertical layers decreasing in stiffness toward a fault core, replicating the variation in stiffness of the fault damage zone (e.g., Gudmundsson, 2011). In this setup, the softest layer is the fault core which is characterized by the lowest value of Young's modulus or stiffness (0.1 GPa); this is surrounded by a fault damage zone which stiffens gradually approaching that of the host rock (40 GPa). For simplicity, here, the damage zone stiffness is assumed constant at any particular time. Fault zone stiffness, however, was varied over time in separate model runs to incorporate the dynamic nature of fault development both syn- and post-collapse. Temporal changes reflect initial fault growth, and subsequent healing and intrusion by dikes. All models simulate snapshots of the magnitudes and directions of principal stress around the pressurized sheet; the likely propagation path is then inferred based on the trajectories of the maximum

Fig. 6 General COMSOL model setup used throughout. In all runs, the models are fastened at the outer boundary using a fixed constraint; this is coupled with an infinite element domain on the inner model margin to ensure the fixed boundary effects do not influence results. The host rock and fault zone are modeled using different values for Young's modulus (E) as specified in the "Model results" section. An inclined sheet is modeled as a cavity with an excess pressure (P_e); sheet angle is varied throughout model runs

principal compressive stress (σ_1). Boundary conditions were used to test the model's response to a simulated vertical normal-fault dip-slip displacement (Fig. 11), modeled as a compressive stress, of 5 MPa applied to the collapsing block, and normal-fault dilation (Fig. 11), modeled as a tensile stress, of 5 MPa applied perpendicular to the fault. Trajectories of the maximum principal compressive stress (σ_1) and the magnitude of the minimum principal compressive stress (σ_3) are shown in all model runs.

Model results

Several numerical models were run with different fault zone setups, generated by varying the mechanical properties (Young's modulus) across the fault. A homogeneous setting, whereby the fault zone shared the same mechanical properties as the host rock, was initially modeled and provided a reference to compare other model results. In this setup, the fault has little or no effect on sheet propagation. Additional model runs are displayed throughout (Figs. 7, 8, 9, 10, and 11).

Several geometrical setups were run by varying the sheet dip angle (θ), to confirm the relative effects of fault zone mechanical heterogeneity against intrusion angle. We observe that shallow-dipping sheets, those with dips less than 45°, do not alter the local fault stress significantly enough to promote deflection or arrest, unless additional boundary conditions are applied (see Fig. 11). In all models, the maximum tensile stress (σ_3) occurs at the sheet tip, and the maximum compressive stress (σ_1), shown as white cones, are used to interpret the likely fracture pathway. All models show stress contours in the range of 0.5–6 MPa, the upper end of this range being the most likely to induce fracturing (Amadei and Stephansson, 1997).

When a mechanical contrast between the fault and host rock is modeled, a rotation of principal stress occurs near the sheet tip and a temporary change in principal stress orientation at the contact between the fault and host rock. In order for the sheet to become deflected into a subvertical dike along the ring fault, as observed in Hafnarfjall, the values of Young's modulus must be sufficiently different between the individual modeled fault zone layers, in order to induce an elastic mismatch. Figure 7 highlights a situation whereby the layers which constitute the fault damage zone are not significantly different from those of the host rock and thus promote neither elastic mismatch nor principal stress rotation. This condition, namely similar elastic properties of the fault zone and the host rock, favors transverse sheet propagation through the fault. In contrast, models shown in Figs. 8 and 9 simulate a more mechanically heterogeneous fault zone, with Young's modulus differing by orders of magnitude. In these situations, sheet deflection is favored due to the mechanical mismatch between the individual layers. The fracture propagation path at the
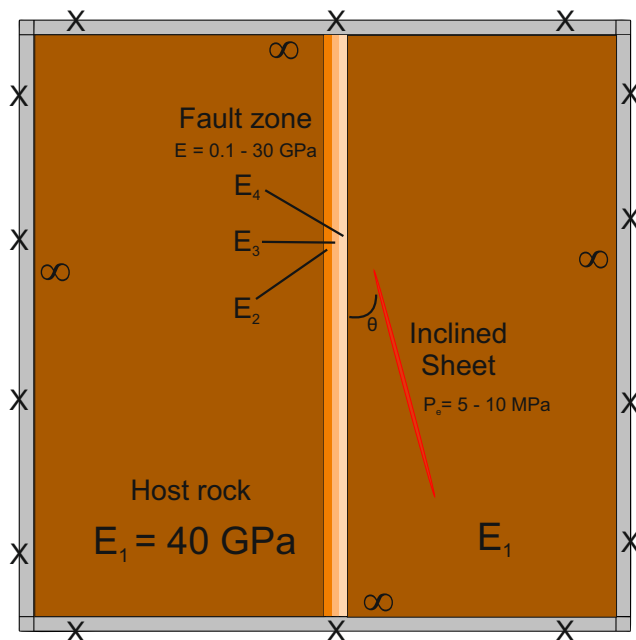
Fig. 7 Young's modulus in the fault zone ranges between 10 and 30 GPa. Sheet dips shown are 45°, 65°, and 75°, and sheet overpressure is 10 MPa. In all models, tensile stress concentrates through the fault plane, indicating that any fracture would likely propagate through the fault. Rotation of the maximum compressive stress (*white cones*) occurs in line with the fault dip for those sheets that dip 65° and greater, suggesting that a fracture may align preferentially with the fault. Large stress shadows are created ahead of fracture tip, as indicated by the absence of stress trajectories
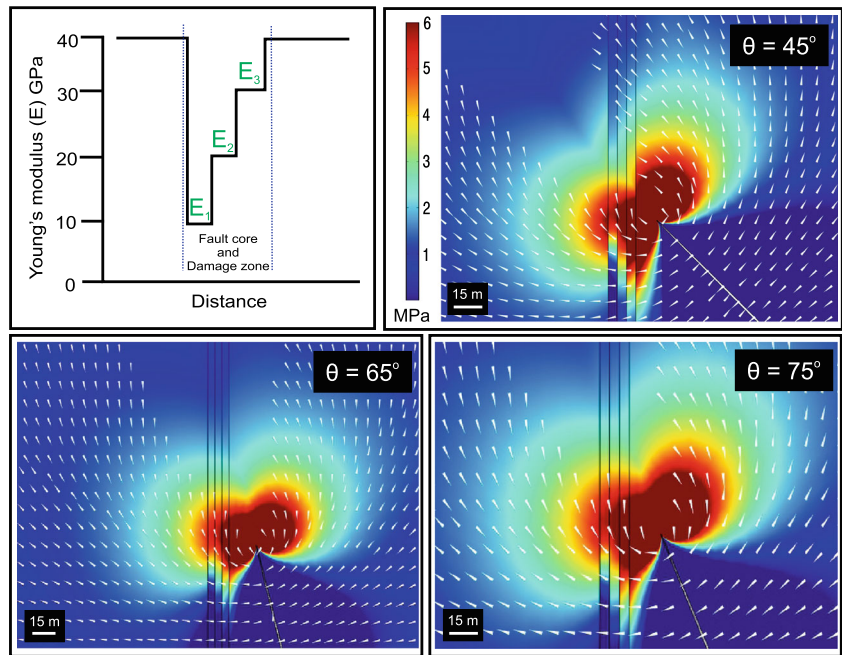
sheet tip is inferred from the trajectories of σ_1 (which the sheet follows), surrounding the sheet and fault zone. It is only when these trajectories rotate to subvertical that the sheet will deflect into a dike within the fault. Such a situation is much more likely in models which simulate a sheet with an initially steep dip (i.e., >65°).

To model the effect of a previously intruded dike in the ring fault, a stiff layer is added to the center of the fault zone (Fig. 10). Such a situation is likely if a lower part of the fault was intruded by a ring dike in the conventional manner described by Anderson (1936) and Walter (2008) or if inclined

sheets were previously captured and deflected (see Appendix 1). The stiff layer creates a clear stress barrier and zone of elastic mismatch, indicating that transverse sheet propagation in this scenario is unlikely. Instead, any sheet would likely become deflected or arrested at the contact between the weak damage zone and the stiff dike (Fig. 10).

Boundary conditions were applied to the model edge to simulate (1) extension across the fault and (2) block subsidence. A compressional stress of 5 MPa was applied to the intra-caldera block (Fig. 11). In this model run, the modeled principal stress axis rotates to subvertical with little

Fig. 8 Young's modulus in the fault zone ranges between 0.1 and 10 GPa, and sheet overpressure is 10 MPa in all models. In all model runs, tensile stress concentrates within the 10-GPa layer closest the sheet. Softer layers suppress most of the tensile stress, and principal stress rotation within the fault core favors vertical sheet deflection. This rotation effect is much less pronounced for those sheets which dip below 60–70°; for example, the 65° model shown displays inclined σ_1 trajectories throughout the vertical fault cross section
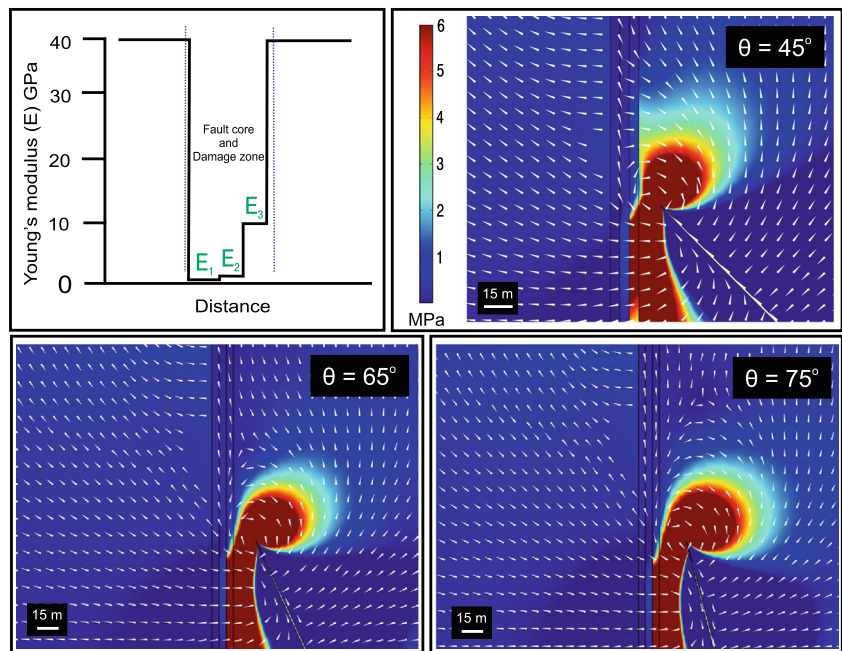
Fig. 9 Fault zone Young's modulus ranges from 1 to 30 GPa, and sheet overpressure is 10 MPa in all models. In models with sheets that dip greater than ~45°, a significant rotation of the maximum compressive stress is observed. **c, d** The trajectories of σ_1 rotate to vertical within the fault, whereas in **b**, trajectories are initially vertical but become inclined higher up the fault
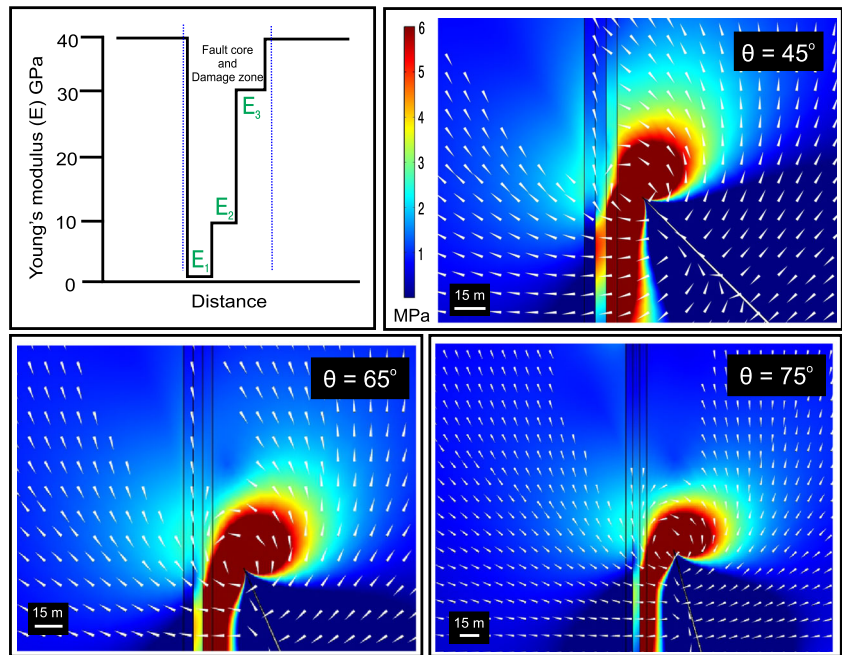
dependence on the angle of the sheet; this situation would favor sheet propagation into and along the plane of the ring fault, thereby allowing magma to propagate in a manner consistent with that interpreted from field observations, although principal stress rotation further up dip of the fault may induce fracture arrest later on. The second boundary condition simulates an extensional force acting perpendicular to the fault, which would likely encourage fault dilation. In these situations, it is much easier for a low-angle sheet to deflect into the fault; in Fig. 11, we show a 35° dipping sheet.

Finally, a model is included to assess the background boundary effects of a magma chamber subject to pressure in excess of lithostatic, a necessary requirement for the propagation of a sheet. In this model (Fig. 12), an 8-km-wide and 1-km-thick sill-like magma chamber is situated in a homogeneous crustal segment at 5-km depth. The magnitude and orientation of stresses highlight the potential for inclined sheet propagation, particularly at the chamber outer margins. Several softer layers were added to the model; these were placed vertically to simulate the caldera fault zones previously

Fig. 10 A stiff layer (40 GPa) is added to the center of the fault zone to simulate a previous dike intrusion. Principal stress rotation at the sheet tip and stress concentration within the stiff layer favor fault capture, most likely along the nearside edge of the previous intrusion. Sheet approach angle has little effect on the stresses within the fault zone above 35°
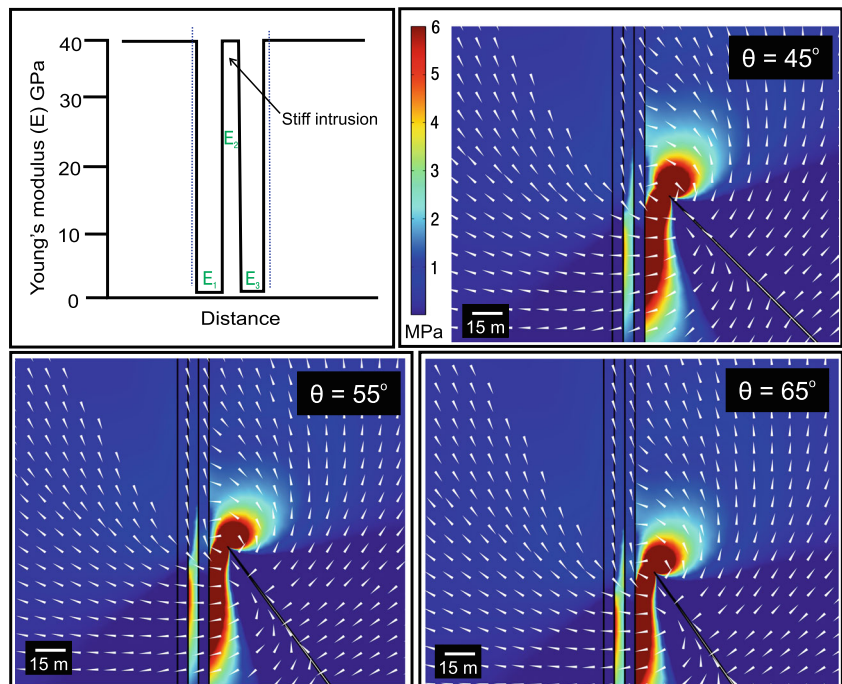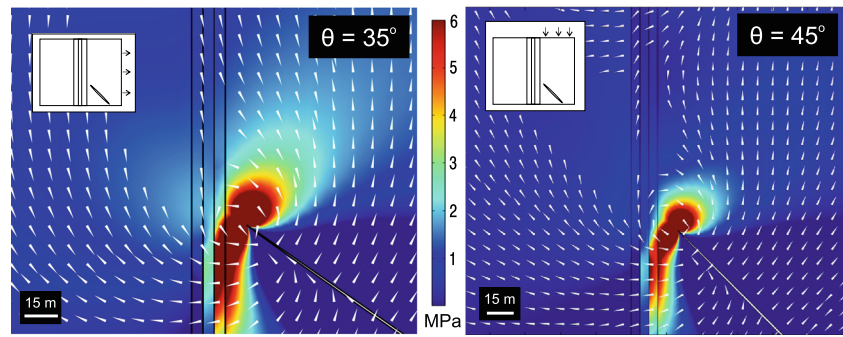
Fig. 11 Models showing the effect of various boundary conditions. Here, a tensile stress (5 MPa) is applied to the far right of the model (**a**) and a compressive stress (5 MPa) to the upper part of the intra-caldera block in the model (**b**)

discussed and horizontally to simulate, in a simple way, mechanical layering in a volcanic edifice. Stresses clearly concentrate within the fault margins in the caldera block, indicating that faults act as stress barriers. There is little principal stress rotation observed at the fault contact, indicating that if the tensile stress was high enough (0.5–6 MPa) to generate a fracture, then the likely propagation path would be through the fault. However, the required stress concentration is rarely met as the inner (core) part of fault tends to suppress stresses.

Once a fault captures an inclined sheet and deflects it into the first subvertical dike, it is generally much easier for subsequent sheets to deflect at the contact between the lava pile and the first dike (Fig. 3). This follows because the stiffness of a vertical intrusion is much greater than that of the area surrounding the fault damage zone, and therefore, principal

stress rotation and elastic mismatch parameters favor dike propagation over continuation of an inclined sheet.

Discussion and conclusions

It is well known that normal faults can alter the propagation pathway of subvertical dikes (Valentine and Krogh, 2006; Gaffney et al., 2007; Ziv and Rubin, 2000) and sills (Magee et al., 2013). Several assumptions and inferences have been made regarding the role of caldera ring faults in channeling magma (Anderson, 1936; Saunders 2001; Jonsson, 2009); the most common mechanical explanation offered to decipher this process relies on magma chamber underpressure (Anderson, 1936). This model suggests that many ring dikes form during
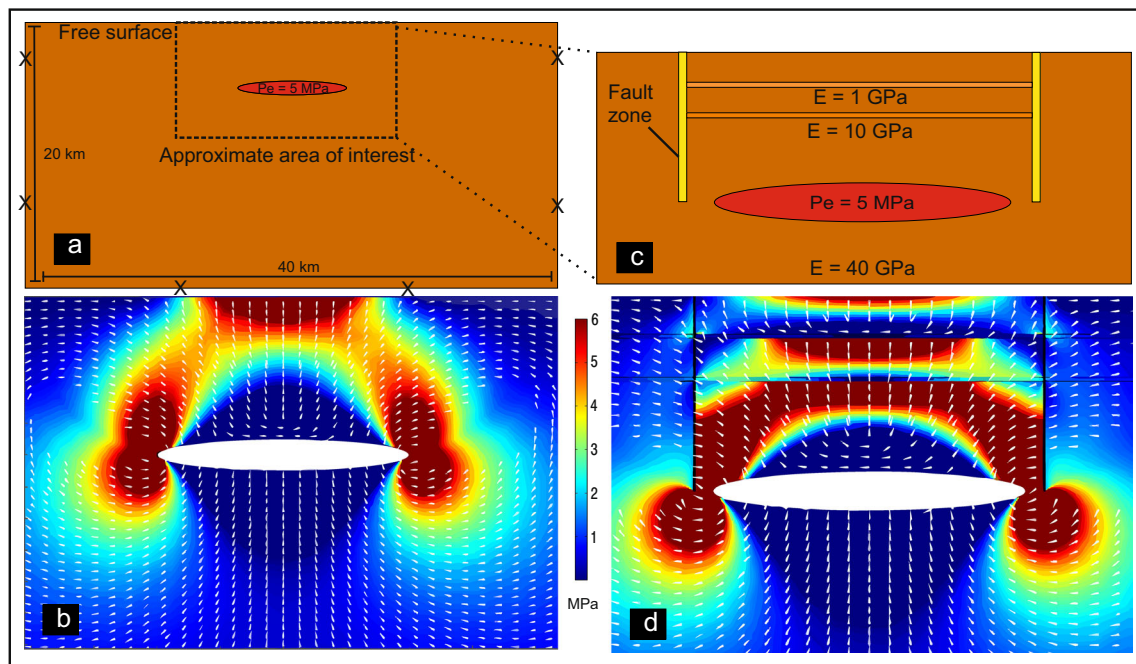

Fig. 12 Background stresses associated with a modeled **a** 8-km-wide and 1-km-thick sill-like magma chamber at 5-km depth with an overpressure of 5 MPa. **b** Principal stresses become oriented in a manner which favors inclined sheet propagation from the chamber margins. **c** Model setup includes a peripheral fault zone, with a lower Young's modulus than the surrounding host rock, as well as two soft horizontal layers at 1- and 2-km depth. **d** Results indicate that the fault acts as a significant stress barrier. Furthermore, the soft horizontal layers act in a similar manner, also exhibiting significant principal stress rotation at the boundary of the uppermost and softest layer

large explosive eruptions, leading to chamber roof collapse and the flow of evolved magmas up into the ring faults. Alternative mechanical models are hampered by the poor availability of data on the structure of ring faults at depth and the lack of detailed observations of the interactions between ring faults and magma.

Here, we present an alternative mechanism of ring dike formation which suggests that some ring dikes do not channel magma directly from the margins of a magma chamber but rather form through inclined sheets being captured and deflected along the ring fault (Fig. 13). This mechanism is in agreement with observations of restless calderas (e.g., Saunders, 2001) and the location of numerous dike-fed eruptive centers, located on ring fault margins (Walker, 1984; Geyer and Martí 2008). However, several caldera volcanoes experience eruptive activity located outside of their ring fault margins, for example the fissure eruptions of Fernandina in 1995 (Chadwick et al., 2011). Our model supports the interpretation that the sheet which fed these fissures had a shallow dip (12–14°) at a depth of ~1 km, near the chamber margin (Chadwick et al., 2011). This follows because sheet deflection is unlikely at dip angles lower than ~45° (see Figs. 7, 8, 9, and 10). Note, also, that many mafic calderas have complex ring fault structures controlled by post-collapse subsidence, for example Colli Albani (Giordano et al., 2006).

Dikes can become arrested and deflected at contacts between layers with mechanical mismatch (contrasting mechanical properties) such as stiff lava flows and compliant (or soft) tuff layers (Gudmundsson, 2011; see Fig. 12). It has been suggested that elastic mismatch and associated local stresses partly control the frequency with which dikes reach the surface to feed eruptions (Gudmundsson and Phillip, 2006). In this view, it is only when the state of stress in a volcanic edifice becomes roughly homogeneous that a dike can propagate to the surface, a condition more likely to be reached in edifices composed of mechanically similar layers. Similarly, if a caldera fault develops a fault core, it may act as a single vertical and roughly homogeneous layer, thereby promoting stress field homogenization and providing a pathway for magma channeling toward the surface.

A large proportion of the world's volcanism occurs within or around active calderas (Newhall and Dzurisin, 1988), and therefore, understanding the control of caldera structures on magma movement is vital for predicting the location and timing of eruptive activity. The caldera fault at Hafnarfjall is one of the best exposures of its kind in the world. It represents a segment of the ring fault, visible as a 200-m vertical exposure. The fault has variable attitude, but overall, it is a steeply inward-dipping normal fault.

Many faults offer potential pathways for magma. However, very steeply dipping faults, such as the ring fault in Hafnarfjall, are perhaps particularly favored paths because the normal stress on steep faults in rifting environments tends to be comparatively small (Gudmundsson, 2011). In this particular case, the ring fault has deflected and acted as a channel for inclined sheet propagation; some of the sheets may have reached the surface to supply magma for eruptions. In addition, the ring fault has captured and deflected inclined sheets to form a ring dike, a mechanism of ring dike formation that has not been reported earlier. These results further underline the importance of understanding magma-fault interaction in relation to volcanic hazards. It is likely that the process of sheet deflection and ring dike formation, described here, provides a major control on the location of resurgent caldera volcanism.
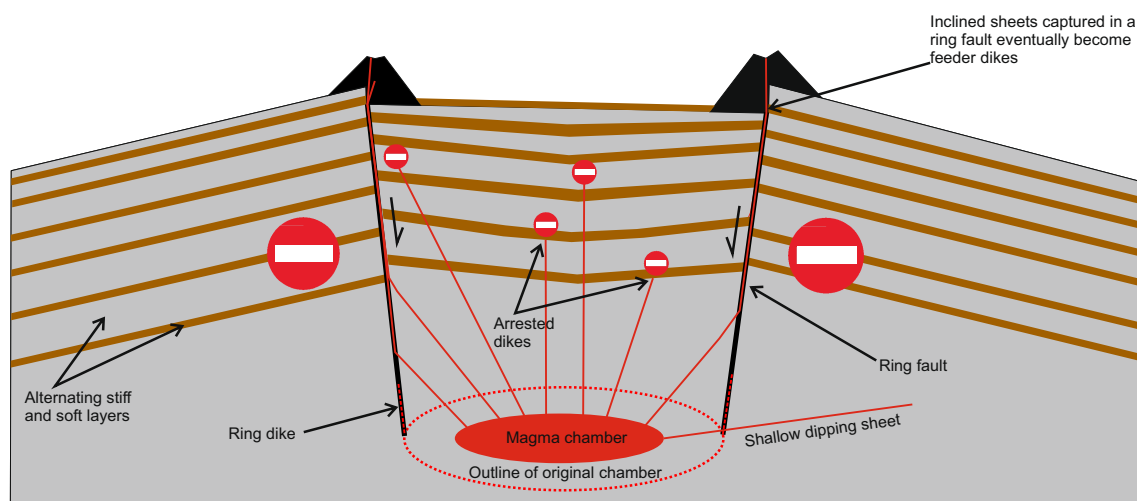

Fig. 13 Conceptual resurgent caldera model. In the model, an edifice is made of layers of contrasting mechanical properties, e.g., stiff lavas and soft tuffs and sediments. A number of dikes fail to reach the surface and become arrested at layer contacts. Inclined sheets propagating from the shallow magma chamber become captured by the ring fault. The ring fault deflects many sheets into subvertical dikes, some of which may have propagated to the surface. Shallow-dipping sheets may penetrate the fault to force eruptions outside of the ring fault margin

References

Acocella V, Cifelli F, Funiciello R (2000) Analogue models of collapse calderas and resurgent domes. J Volcanol Geotherm Res 104:81–96

Acocella V (2007) Understanding caldera structure and development: an overview of analogue models compared to natural calderas. Earth Sci Rev 85:125–160

Amadei B, Stephansson O (1997) Rock stress and its measurement. Chapman and Hall, New York

Anderson EM (1936) The dynamics and formation of cone-sheets, ring-dikes, and cauldron-subsidence. R Soc Edinb Proc 128–157

Anderson TL (2005) Fracture mechanics: fundamentals and applications, 3rd edn. Taylor & Francis, London, p 621

Bedard JH, Naslund HR, Nabelek P, Winpenny A, Hryciuk M, Macdonald W, Hayes B, Steigerwaldt K, Hadlari T, Rainbird R, Dewing K, Girard E (2012) Fault-mediated melt ascent in a Neoproterozoic continental flood basalt province, the Franklin sills, Victoria Island, Canada. Geol Soc Am Bull 124:723–736

Branney MJ (1995) Downsag and extension at calderas: new perspectives on collapse geometries from ice-melt, mining, and volcanic subsidence. Bull Volcanol 57:303–318

Burchardt S, Walter TR (2010) Propagation, linkage, and interaction of caldera ring-faults: comparison between analogue experiments and caldera collapse at Miyakejima, Japan, in 2000. Bull Volcanol 72: 297–308

Chadwick WW, Jonsson S, Geist D, Poland M, Johnson DJ, Batt S, Harpp KS, Ruiz A (2011) The May 2005 eruption of Fernandina volcano, Galapagos: the first circumferential dike intrusion observed by GPS and InSAR. Bull Volcanol 73:679–697

Clough CTH, Maufe HB, Bailey EB (1909) The cauldron subsidence of Glen Coe and the associated igneous phenomena. Q J Geol Soc Lond 65:611–678

Delaney PT, Pollard DD, ZIony JI, McKee EH (1986) Field relations between dikes and joints: emplacement processes and paleostress analysis. J Geophys Res 91:4920–4938

Ekstrom G (1994) Anomalous earthquakes on volcano ring-fault structures. Earth Planet Sci Lett 128:707–712

Franzson H (1978) Structure and petrochemistry of the Hafnarfjall_Skardsheidi central volcano and the surrounding basalt succession, W-Iceland [Ph.D. thesis]: Edinburgh, Scotland, university of Edinburgh 264 pp

Gaffney ES, Damjanac B, Valentine GA (2007) Localization of volcanic activity: 2. Effects of pre-existing structure. Earth Planet Sci Lett 263:323–338

Gautneb H, Gudmundsson A, Oskarsson N (1989) Structure, petrochemistry and evolution of a sheet swarm in an Icelandic central volcano. Geol Mag 126:659–673

Geyer A, Folch A, Martí J (2006) Relationship between caldera collapse and magma chamber withdrawal: an experimental approach. J Volcanol Geotherm Res 157:375–386

Geyer A, Marti J (2014) A short review of our current understanding of the development of ring faults during collapse caldera formation. Front Earth Sci 2:22. doi:10.3389/feart.2014.00022

Geyer A, Martí J (2008) The new worldwide collapse caldera database (CCDB): a tool for studying and understanding caldera processes. J Volcanol Geotherm Res 175:334–354

Geshi N, Shimano T, Chiba T, Nakada S (2002) Caldera collapse during the 2000 eruption of Miyakejima volcano, Japan. Bull Volcanol 64:55–68

Giordano G, De Benedetti AA, Diana A, Diano G, Gaudioso F, Marasco F, Miceli M, Mollo S, Cas RAF, Funiciello R (2006) The Colli Albani mafic caldera (Roma, Italy): stratigraphy, structure and petrology. J Volcanol Geotherm Res 156:49–80

Gudmundsson A (1998) Formation and development of normal-fault calderas and the initiation of large explosive eruptions. Bull Volcanol 60:160–170

Gudmundsson A, Nilsen K (2006) Ring-faults in composite volcanoes: structures, models and stress fields associated with their formation. Geol Soc Lond, Spec Publ 269:83–108

Gudmundsson A, Berg SS, Lyslo KB, Skurtveit E (2011) Fracture networks and fluid transport in active fault zones. J Struct Geol 23:343–353

Gudmundsson A (2011) Rock fractures in geological processes. Cambridge University Press, Cambridge. doi:10.1017/CBO9780511975684

Gudmundsson A, Phillip SL (2006) How local stress fields prevent volcanic eruptions. J Volcanol Geotherm Res 158:257–268

Hardy S (2008) Structural evolution of calderas: insights from two-dimensional discrete element simulations. Geology 36:927

He MY, Hutchinson JW (1989) Crack deflection at an interface between dissimilar elastic materials. Int J Solids Struct 31:3443–3455

He MY, Evans AG, Hutchinson JW (1994) Crack deflection at an interface between dissimilar elastic materials. Int J Solids Struct 25:1053–1067

Holohan EP, Troll VR, Walter TR, Münn S, McDonnell S, Shipton ZK (2005) Elliptical calderas in active tectonic settings: an experimental approach. J Volcanol Geotherm Res 144:119–136

Holohan, EP., Walter, TR., Schöpfer, MPJ., Walsh, JJ., van Wyk de Vries, B. and Troll, VR. (2013). Origins of oblique-slip faulting during caldera subsidence. J Geophys Res Solid Earth, No. 2, p. n/a–n/a

Jaeger JC, Cook NGW (1979) Fundamentals of rock mechanics. Chapman and Hall, London

Johannesson H (1975) Structure and petrochemistry of the Reykjadalur central volcano and surrounding areas, midwest Iceland. PhD Thesis, University of Durham, Durham, 273 pp

Johnson SE, Schmidt KL, Tate MC (2002) Ring complexes in the Peninsula Ranges Batholith, Mexico and the USA: magma plumbing systems in the middle and upper crust. Lithos 61: 187–208

Jonsson S (2009) Stress interaction between magma accumulation and trapdoor faulting on Sierra Negra volcano, Galapagos. Tectonophysics 471:36–44

Kennedy B, Stix J, Vallance JW, Lavallée Y, Longpré MA (2004) Controls on caldera structure: results from analogue sandbox modeling. Geol Soc Am Bull 116:515

Kokelaar P (2007) Friction melting, catastrophic dilation and breccia formation along caldera superfaults. J Geol Soc 164:751–754

Lipman, PW (1984) The roots of ash flow calderas in Western North America: Windows into the tops of Granitic batholiths. J Geophys Res 89:8801–8841

Lipman PW (1997) Subsidence of ash-flow calderas: relation to caldera size and magma chamber geometry. Bull Volcanol 59:198–218

Magee C, Jackson CAL, Schofield N (2013) The influence of normal fault geometry on igneous sill emplacement and morphology. Geology 41:407–410

Michon L, Villeneuve N, Catry T, Merle O (2009) How summit calderas collapse on basaltic volcanoes: new insights from the April 2007 caldera collapse of Piton de la Fournaise volcano. J Volcanol Geotherm Res 184:138–151

Newhall CG, Dzurisin D (1988) Historical unrest at large calderas of the world. US Geol Sur Bull 72:85–100

Saunders ST (2001) The shallow plumbing system of Rabaul caldera: a partially intruded ring fault? Bull Volcanol 63:406–420

Saunders ST (2004) The possible contribution of circumferential fault intrusion to caldera resurgence. Bull Volcanol 67:57–71

Smith RL, Bailey RA (1968) Resurgent cauldrons. Geol Soc Am Mem 116:613–662

Sparks RSJ (1988) Petrology and geochemistry of the Loch Ba ring-dike, Mull (NW Scotland): an example of the extreme differentiation of theolitic magmas. Contrib Mineral Petrol 100:446–461

Troll V, Walter TR, Schmincke HU (2002) Cyclic caldera collapse: piston or piecemeal subsidence? Field and experimental evidence. Geology 30:135–138. doi:10.1130/0091-7613(2002)030<0135

Tucker D, Hildreth W, Ullrich T, Friedman R (2007) Geology and complex collapse mechanisms of the 3.72 Ma Hannegan caldera, North Cascades, Washington, USA. Geol Soc Am Bull 119:329–342. doi:10.1130/825904.1

Valentine GA, Krogh KEC (2006) Emplacement of shallow dikes and sills beneath a small basaltic volcanic center—the role of pre-existing structure (Paiute Ridge, southern Nevada, USA). Earth Planet Sci Lett 246:217–230

Walker GPL (1960) Zeolite zones and dike distribution in relation to the structure of the basalts of eastern Iceland. J Geol Soc 68:515–527

Walker GPL (1984) Downsag calderas, ring faults, caldera sizes, and incremental growth. J Geophys Res 89:8407–8416

Walter TR (2008)Facilitating dike intrusions into ring-faults. In: Gottsmann J, Joan Martí (eds) Caldera volcanism: analysis, modelling and response, vol 10. Elsevier, Heidelberg, pp 351–374

Walter TR, Troll VR (2011) Formation of caldera periphery faults: an experimental study. Bull Volcanol 63:191–203

Wang P, Xu LR (2006) Dynamic interfacial debonding initiation induced by an incident crack. Int J Solids Struct 43(21):6535–6550

Xu LR, Huang YY, Rosakis AJ (2003) Dynamic crack deflection and penetration at interfaces in homogeneous materials: experimental studies and model predictions. J Mech Phys Solids 51:461–486

Ziv A, Rubin AM (2000) Stability of dike intrusion along pre-existing fractures. J Geophys Res 105